Depth dependence of vacancy formation energy at (100), (110), and (111) Al surfaces: A first-principles study

S. S. Gupta,[1,*] M. A. van Huis,[1] M. Dijkstra,[1] and M. H. F. Sluiter[2]

[1]*Soft Condensed Matter, Debye Institute for Nanomaterials Science, Utrecht University, Princetonplein 5, 3584 CC Utrecht, The Netherlands*

[2]*Department of Materials Science and Engineering, Delft University of Technology, Mekelweg 2, 2628 CD Delft, The Netherlands*

(Received 2 December 2015; published 19 February 2016)

Vacancy defects are known to play an important role in the structural and chemical properties of metallic and semiconductor nanoparticles. Here, we investigate the likelihood of vacancy formation at the surface, in the subsurfaces, and in the interior of a model system of Al nanocrystals. The depth dependence of the vacancy formation energy (VFE) in 14–17 layered low-indexed surfaces of aluminium is studied using LDA, PBE, and PBEsol exchange-correlation functionals. Within a depth of two subsurface layers, the functionals make a transition from a similar description of surfaces to the differences in VFEs observed in bulk Al. The VFE converges to the bulk value within 0.01 eV beyond a maximum depth of 3–6 atomic layers, depending on the crystallographic surface plane. We find that the different convergence behaviors are related to the relaxations of atomic planes, normal to the surface, which in turn depend on the packing density of these surfaces. For the (111) subsurfaces, surprisingly, the defect formation energies are found to be higher than that of bulk Al, which is related to the hindered relaxations in its close-packed atomic planes. Although our results predict considerably lower VFE for the topmost layers of all the surfaces, the likelihood of forming a vacancy in the immediate subsurfaces of multifaceted Al nanoparticles is predicted to be lower than in bulk Al, which is in contrast to expectation.

DOI: 10.1103/PhysRevB.93.085432

I. INTRODUCTION

Vacancies occurring at the surfaces and subsurfaces can influence materials' chemical reactivity, mechanical strength, and may cause thermodynamic processes such as surface roughening and diffusion at elevated temperatures [1–6]. With the rapid developments taking place in the nanosciences, whereby the nanocrystals are synthesized and post-processed with several physical and chemical treatments, the formation of such defects poses an important subject for investigation. The presence of vacancy defects on the surfaces of metallic or compound semiconductor nanocrystals can alter the electronic surface states, which further may result into magnetically, optically, or catalytically active sites, or may even facilitate processes such as ion exchange [6–8]. The occurrence of these defects depends on the temperature, and their formation energies and entropies. Here, we study the vacancy formation energy (VFE) in the low-indexed Al surfaces where the defect environment is varied from that of a surface to a bulklike interior.

Here we present a systematic *ab initio* study to determine the convergence behaviors of VFEs from surface to bulk values, for different crystallographic surfaces. Previous studies using density functional theory were reported for vacancy defects on only Al(111) [9,10] and Pd(111) [11] by using slabs of 5–7 atomic layers. Other studies on monovacancy defect formation on Al [12,13] and Cu(001) [14] surfaces used semiempirical potentials. In this work, we use aluminium as our prototype metal to investigate the energetics of vacancy formation on, and beneath, the (100), (110), and (111) crystallographic surfaces. By using slabs comprising of 14–17 atomic layers as a model for surfaces, we establish well-converged surface characteristics by relaxing all the atoms. We examine surface energies, interplanar relaxations, and compare the VFE convergence to bulk values using the local density approximation (LDA) [15,16], generalized gradient approximation of Perdew, Burke, and Ernzerhof (GGA-PBE) [17], and its revised version for solids (PBEsol) [18]. We understand these convergence trends by analyzing the relaxations of the nearest neighbors of the defective sites, perpendicular to the surface, thus, highlighting their role in the VFE convergence. The results for different functionals reveal how a similar description of surfaces branches out into different VFEs of bulk Al, within a depth of two subsurface layers. With a nonintuitive and nonmonotonous convergence trend seen in Al(111), this work also opens up the question whether vacancies are very likely to occur in the immediate subsurfaces of aluminium nanocrystals, and how that may depend on the different crystallographic facets of these crystals.

II. METHODS

First-principles density functional theory (DFT) calculations are performed using Vienna *ab initio* simulation package (VASP 5.3.5) [19–21], where the single-electron wave functions and projector augmented-wave potential sets [22] are expanded using a plane-wave basis. For a convergence within 0.5 meV/atom, an energy cutoff of 400 eV for the plane waves and 560 eV for the augmentation charges was found to be sufficient. The electronic states and the potentials were sampled from the first Brillouin zone by using a weighted-grid-based scheme of Monkhorst and Pack [23], with a Methfessel-Paxton smearing of 0.2 eV [24]. The sampled **k** mesh for bulk calculations was set sufficiently dense such that (number of **k**

*s.s.gupta@uu.nl

points)×(number of atoms in the supercell) > 10 000. Specifically for the bulk supercells containing 32 and 108 atoms, Γ-point centered $7 \times 7 \times 7$ and $5 \times 5 \times 5$ **k** meshes were used, respectively. For these bulk calculations, we studied monovacancies and divacancies using the LDA, PBE, and PBEsol functionals. These exchange-correlation functionals were also used for studying the monovacancies in the low-indexed Al surfaces. Only for a comparison with other functionals, we have also used the AM05 functional [25] for pure and defective bulk Al. This functional was developed within the subsystem functional approach where (in AM05) the exchange part includes the LDA exchange and surface effects of an Airy gas model [26], and the correlation part includes a LDA part and a scaling factor fitted to the jellium surface exchange-correlation energies. For the case of bulk Al, AM05 overestimates the defect formation energies; hence, it is not considered further for the study of pure or defective Al surfaces.

In this study we have not used any previously derived schemes [27,28] to correct the errors caused by long-range elastic strain associated with the point defects in finite bulk supercells. This is because these corrections could be implemented only if they are consistently used for the bulk and surface supercells; however, an analog correction scheme for the defective surface supercells is not yet understood. Also, the errors in treating the evanescent nature of the electron density around a point defect are not corrected here within any known schemes [29–32], which account for the internal surface of the defect. Due to the nontrivial defect areas arising on different crystallographic surfaces and subsurface depths, the corrections devised by Mattson and co-workers [29–31] are not extendable. Also, the intrinsic surface correction per unit area $\sigma_{cor}^{xc}[n(r)]$ for the PBEsol functionals is not known, which restricts the use of the correction scheme proposed in [32]. We believe our analysis which does not directly address such errors, in the least, still ensures that these are systematically contained by considering the same concentration of defects for all the surface calculations. This qualifies one to make comparisons of relative trends in VFEs for different low-indexed Al surfaces.

III. RESULTS AND DISCUSSION

A. Pure bulk

To understand the energetics of vacancy formation on Al surfaces, it is imperative to study the defects relative to the bulk system. For this, we calculated the structural properties of face-centered-cubic (fcc) bulk Al such as lattice parameter a, bulk modulus B, and cohesive energy E_{coh}. The results for various functionals are reported and compared in Table I. The lattice parameter is derived from the total energy minimum for a range of unit-cell volumes, while the bulk modulus is calculated by fitting this equation of state with the universal model derived in [33]. A spin-polarized, orbital constrained calculation was used to generalize the functional of the Al atom for the calculation of cohesive energy E_{coh}. These cohesive energy predictions are generally compared by the 0-K extrapolation of the sublimation energies obtained using low-temperature experiments.

TABLE I. Bulk-Al properties such as lattice parameter a, bulk modulus B, and cohesive energy E_{coh}, calculated for different exchange-correlation functionals.

	LDA	PBE	PBEsol	AM05
a (Å)				
This study	3.984	4.039	4.016	4.007
Others	3.98 [37]	4.04 [31,37,38]	4.013 [35]	4.0076 [39]
Expt.		4.02 [35], 4.022 [34]		
B (GPa)				
This study	84.6	77.6	82.5	86.7
Others	84 [31,37]	78 [31,37]	82.6 [35]	84.8 [36]
Expt.		81.3 [34]		
E_{coh} (eV)				
This study	3.98	3.47	3.82	3.73
Others	4.01 [40]	3.43 [35,40]	3.81 [40]	
Expt.		3.39 [41], 3.43 [34]		

Table I shows that among the chosen exchange-correlation functionals, LDA and PBE, respectively, mark the lower and upper bounds in predicting the Al lattice parameter. The experimental values of lattice parameter and bulk modulus are referred from [34], where the effect of finite temperature and zero-point phonon effects are included. These values are most suitable to compare with the first-principles results of this study. For the bulk modulus, PBEsol predictions are in excellent agreement with the experimental results in [34]. As known in the literature, AM05 and PBEsol functionals are seen to predict very similar structural bulk properties [35,36]. This is understandable as these two functionals are constructed by fitting to the exchange-correlational energies of the jellium surface model, although through different approaches. For $E_{coh.}$, PBE gives excellent agreement with experiments as it is well suited for describing the atomic and molecular species. As a typical feature of the LDA functional, its cohesive energies are seen to be severely overestimated.

B. Vacancy defects in bulk

After studying the bulk properties of fcc Al using various functionals, a simple vacancy defect was introduced by removing one of the atoms from the supercell. While modeling such monovacancies within periodic boundary conditions, it is important that the interaction of the defect and its periodic image is limited. To reduce such errors, we studied the vacancy defects for $3 \times 3 \times 3$ supercells, containing 108 atoms. The calculations in the bulk supercells were performed under two cases: at constant volume and constant pressure ($P = 0$) conditions. In the latter case, along with the ionic positions the cell shape and the cell volume were also relaxed. The two sets of calculations would converge to the same value of VFE in the limit of very low concentration. In our study, these calculations for monovacancies converge within a difference of ∼5 meV for all the exchange-correlation functionals. This indicates that the cell size provides a reasonable convergence of VFE for the concentration of defects considered here.

TABLE II. Vacancy formation and binding energies (eV) in bulk Al, using different exchange-correlation functionals for a supercell of 108 atoms.

	LDA	PBE	PBEsol	AM05
E^f_{vac}				
This study	0.68	0.63	0.74	0.89
Others	0.68 [31]	0.63 [31]	0.75 [42]	0.89 [42]
Expt.		0.67±0.03 [45]		
E^f_{divac}				
This study	1.45	1.33	1.55	1.82
Others	1.48 [44]	1.19 [44]		
Expt.				
E^{bind}_{divac}				
This study	−0.08	−0.08	−0.07	-0.04
Others	−0.07 [44]	−0.08 [44]		
Expt.				

We study the monovacancy and divacancy energetics in bulk Al using Eqs. (1) and (2):

$$E^f_{(n_v)vac} = E_{(N-n_v,n_v)} - \left(\frac{N-n_v}{N}\right)E_{(N,0)}, \quad (1)$$

$$E^{bind}_{divac} = 2E^f_{vac} - E^f_{divac}, \quad (2)$$

where $E^f_{(n_v)vac}$ is the formation energy of n_v vacancies, $E_{(N-n_v,n_v)}$ is the total energy of a defective cell containing $N-n_v$ atoms and n_v vacancies, $E_{(N,0)}$ is the total energy of a perfect cell containing N atoms, and E^{bind}_{divac} are the binding energies of divacancies derived from the formation energies of monovacancies E^f_{vac} and divacancies E^f_{divac}.

The results in Table II are for defective bulk supercells using LDA, PBE, PBEsol, and AM05 functionals. The latter two functionals were constructed with an aim to improve the treatment of surfacelike evanescent charge density variations, by fitting to the exchange-correlation energies of the jellium surface model but using different approaches. In spite of the excellent similarity in predicting the bulk-Al lattice parameter, AM05 and PBEsol exhibit differences in their predictions of the monovacancy formation energy. This is illustrated in detail in Delczeg *et al.* [42] where it is shown that this difference results from the nature of enhancement factors of the two functionals in the high-density regime suitable for aluminium. Due to the severe overestimation of VFE by AM05 it has not been further used in this work for studying the defects on Al surfaces; instead, the LDA, PBE, and PBEsol functionals are used. Also, the experimental values of VFEs shall be referred with care, as they are generally derived by assuming the Arrhenius behavior of the experimental data, which may break down due to local anharmonic effects [43].

All the functionals predict a negative binding energy using Eq. (2) for the divacancies in bulk Al, indicating that divacancies are unstable. The negative binding energy of the divacancies has been explained in detail in Carling *et al.* [44], demonstrating a significant increase in the force constant among the first nearest neighbors of the monovacancy in bulk Al. Unlike the formation energies, the binding energies of divacancies for all the exchange-correlation functionals are seen to be very similar to each other. This is explained in [29], as the surface correction terms in calculating the E^{bind}_{divac} would nearly cancel out, thus, implying that the differences in the VFE for different functionals are mainly due to the electronic part, and not the structural differences like lattice parameters and ionic relaxations. It should be noted that we have studied the divacancies only for bulk supercells, and not for the Al surfaces. This is because to practically consider the low concentration of divacancies in an atomic layer laterally very large supercells would be required, which are beyond the scope of this study.

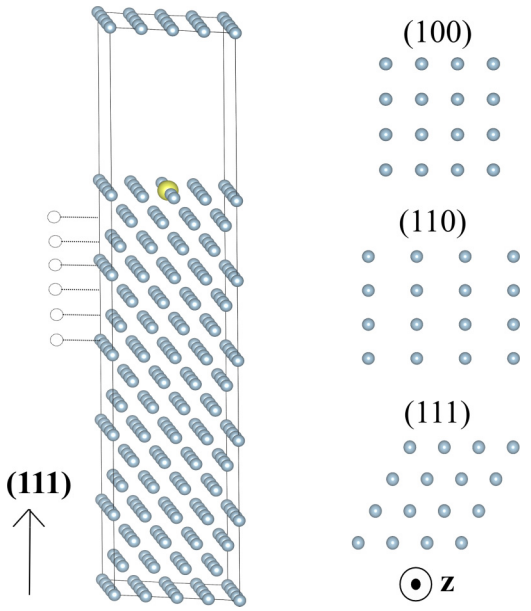

FIG. 1. Left: schematic of a 16-layered (111) slab supercell used for this study. For the depth-dependent profile of VFEs a single monovacancy (marked in yellow and dotted spheres) is created on the surface, and later introduced in the deeper subsurfaces. Right: view from the top of the topmost layer of the three surfaces indicating the differences in the planar packing density in (100), (110), and (111) surfaces.

C. Pure surface

We use the slab model of surface supercells as it enables the study of well-defined crystallographic surfaces and large length scales (∼ nm). In close-packed metals, it is known that about 13 atomic layers are reasonably sufficient for the convergence of interplanar relaxations and surface energies [46]. Our calculations are carried out with 14–17 layered slabs containing 16 atoms per atomic layer, with a vacuum of ∼16 Å, and lateral dimensions of ∼11 Å. A schematic figure of a (111) supercell can be seen in Fig. 1. While keeping the volume of the cell constant, all the atoms were relaxed within a force of 0.01 eV/Å. The **k**-point sampling [23] is done using a mesh of $8 \times 8 \times 1$.

1. Surface energy

One important quantity to investigate through *ab initio* calculations is the surface energy of a given crystallographic surface, as it is not accurately accessible through experiments.

In general, the surface energies can inform about the equilibrium shape of nanocrystals [47] and reactivity of different surfaces for various surface phenomena [48]. The surface energy can be defined as the energy required per unit area, to create a given surface from the bulk crystal. In our calculations it is given by Eq. (3):

$$\gamma(J/m^2) = \lim_{N\to\infty} \frac{1}{2A}\left(E^N_{\text{slab}} - N E^{\text{atom}}_{\text{bulk}}\right), \tag{3}$$

where A is the area, E^N_{slab} is the total energy of a N-atom slab, and $E^{\text{atom}}_{\text{bulk}}$ is the energy per atom in the bulk system.

Before discussing our surface energy results, it should be recalled that LDA is long known to coincidentally give good predictions for the jellium surface energies due to cancellations of errors in the surface exchange and correlation energy components. However, in the case of PBE, there is no such error cancellation, which results in severely underestimating the surface energies [49,50]. To improve upon the deficiencies of PBE, it was revised by Perdew and co-workers [18] by fitting a better agreement with jellium surface, and was later shown to be suitable for solids and surfaces [35,36]. As our study considers the above three functionals for studying vacancy defects, where the defect environment systematically varies from a surface to a bulklike interior, it can provide insights of the performance of these functionals for Al surfaces and bulk Al. This aspect will be covered in detail in Sec. III E.

We have applied the method proposed by Fiorentini *et al.* [53], and further validated by other studies [37,46], to ensure the convergence of surface energies with the number of atomic layers. To overcome the mismatch of bulk and surface calculations, this method separately calculates $E^{\text{atom}}_{\text{bulk}}$ for each crystallographic surface supercell. In the limit of large N, $E^{\text{atom}}_{\text{bulk}}$ is equivalent to the slope of the linear relationship of the total energy of a slab $E^{N_i}_{\text{slab}}$ and N_i atoms, where i is the number of atomic layers. This value of $E^{\text{atom}}_{\text{bulk}}$ is finally used to calculate γ using the limiting case of Eq. (3). The results of surface energies for the three functionals are shown in Fig. 2 and Table III. The inset of Fig. 2 shows the total energy of the slabs $E^{N_i}_{\text{slab}}$ clearly as a linear function of the number of atoms N_i, indicating that the surfaces are thick enough to use the limiting definition of Eq. (3). Among all the surfaces, Fig. 2 shows that (110) being the rough surface with largest relaxations, exhibits convergence within $\sim$0.02 J/m^2. The predictions of surface energy made here use a relatively larger number of atoms than earlier reported in the literature, making our predictions more appropriate for the limiting assumption of large N.

Figure 2 and Table III show that the sequence of the surface energies for all the tested functionals is (111) $<$ (100) $<$ (110), in agreement with the general trend seen in close-packed metals due to the order of bond deficiency on these surfaces. To indicate the relevance of the surface energy values, we have generated an equilibrium shape of an Al nanocrystal ($\sim$5250 atoms) using a commonly used method of Wulff construction [54,55] as shown in Fig. 3. Like most of the fcc metal nanocrystals, the Wulff crystal for Al is a truncated octahedron. Figure 3 highlights that a large part of the surface comprises of (111) and (100) facets, underlying their importance for this study of VFE on Al surfaces. The (110) facets, though not abundant in the morphology, emerge at the edges of (111) facets and may have a role to play in initiating the growth and diffusion mechanisms on these crystals.

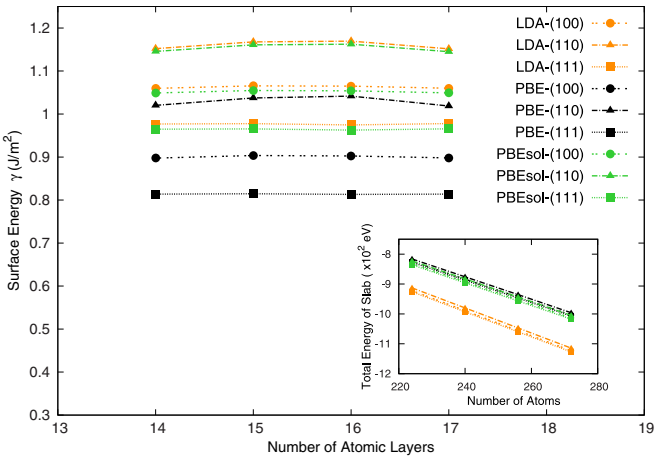

FIG. 2. Surface energies of (100), (110), and (111) Al surfaces are shown for 14–17 layered slabs, using the LDA, PBE, PBEsol functionals. These energies are calculated assuming the limiting case of Eq. (3), where $E^{\text{atom}}_{\text{bulk}}$ is derived by fitting the slope for the linear relation of total energy of these slabs $E^{N_i}_{\text{slab}}$ and the number of atoms N_i. The inset shows the $E^{N_i}_{\text{slab}}$ vs N_i plot for all the considered exchange-correlation functionals. Lines are used to guide the eye.

The results in Fig. 2 and Table III also clearly show that with respect to the LDA and PBEsol surface energy predictions the PBE predictions are significantly lower; the PBE (110) surfaces have about the same surface energy as the LDA (100) and PBEsol (100) surfaces. Consistently, it is seen that predicted surface properties of LDA are almost identical to that of PBEsol functional; however, their behavior in bulk is significantly different as is clear from Table II. Such a similarity of PBEsol and LDA surfaces is in agreement with the enhancement factor analysis in [18] and the predictions of surface energies in [36]. This similarity is again observed while considering defects on these surfaces, and will be discussed in Sec. III E.

2. *Interplanar spacing*

We also analyzed the percentage change in the interplanar spacing $\Delta d_{i,i+1}$ (%) for pure (110) and (111) surfaces, where

TABLE III. Surface energies $\gamma(J/m^2)$ of (100), (110), and (111) surfaces, calculated for different functionals using 14–17 layered slabs.

$\gamma(J/m^2)$	(100)	(111)	(110)
PBE[a]	0.90	0.81	1.03
PBEsol[a]	1.05	0.96	1.15
LDA[a]	1.06	0.98	1.16
Others (LDA)	0.86 [46]	0.67 [46]	0.93 [46]
		0.75 [37]	
		0.83 [51]	
Expt.[b]		1.16 [52]	

[a]This study.
[b]Reported experimental studies in [52] are liquid surface-tension results extrapolated to 0 K.

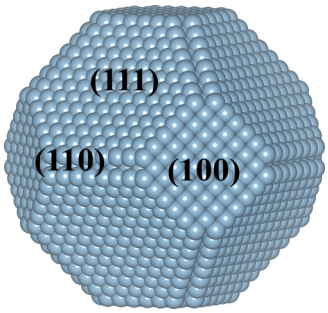

FIG. 3. The Wulff-plot for Al nanocrystal containing ∼5250 atoms is shown, indicating the largely exposed (111) and (100) facets.

i is the layer number. Studying these two surfaces would also indicate the range of behavior for the intermediatelike (100) surface. Historically, Al surfaces have played an important role in understanding the multilayer relaxations of metal surfaces [56–59]. The magnitude of these relaxations is inversely proportional to the packing density of the surface. In general, it is observed that the metal surfaces relax such as to smoothen the electron density at the surface, whereby the steric interactions inherent to a surface orientation determine the degree of these relaxations [56–58].

Figure 4 shows the interlayer relaxations $\Delta d_{i,i+1}$ plotted as a function of the slab depth which is measured by $z_{\text{eff.}}/a_o$, where $z_{\text{eff.}}$ is the distance of the midpoint of the two consecutive atomic layers from the surface and a_o is the lattice parameter. In the top inset of Fig. 4, large and oscillatory relaxation in the interlayer spacing of 16-layer (110) slab is shown, which is also seen in the low-energy electron diffraction (LEED) data [60] and understood by theoretical models [56,57]. The flat surface of Al(111) is seen to undergo very limited relaxations ($\Delta d_{i,i+1} \sim 1\%$) due to the high packing density, shown in the bottom inset of Fig. 4. The insets of Fig. 4 for (110) and (111) surfaces show that these relaxations of the interplanar spacing predicted using the three functionals are very similar, thus, indicating that the differences in describing a surface are mainly due to the differences in treating the electron density near the surface and not the displacements of the ions therein. In the main body of Fig. 4, relaxations $\Delta d_{i,i+1}$ were plotted for slabs with 14–17 atomic layers for the (110) surface, using the PBE functional. The convergence of $\Delta d_{i,i+1}$ for the (110) slabs varies within 1.5%, reflecting the slight spread observed in the surface energies of (110) surfaces, as shown in Fig. 2. Nevertheless, for rough surfaces like (110), where large relaxations would occur, such spread in the surface characteristics could be expected. The reasonable convergence seen in Fig. 4 for varying (110) slab thickness indicates that the number of atomic layers comprising a slab are adequate for studying a physical quantity as a function of depth. In the subsequent sections, we study the VFEs as a function of depth from the free surfaces.

D. Vacancy defects on surfaces

Vacancy defects on these surfaces are studied by creating a monovacancy in one of the subsurface layers of the slab, as seen in Fig. 1. The VFEs on these surfaces, $E^{\text{s}}_{\text{form}}$, can be calculated using Eq. (4):

$$E^{\text{s}}_{\text{form}} = E^{\text{s}}_{\text{vac}}(N-1,1) - E^{\text{s}}_{\text{perf}}(N,0) + E^{\text{atom}}_{\text{bulk}}. \quad (4)$$

Here, the index "s" refers to the surface supercells, $E^{\text{s}}_{\text{vac}}(N-1,1)$ is the total energy of a slab containing $N-1$ atoms and one vacancy, $E^{\text{s}}_{\text{perf}}(N,0)$ is the total energy of a perfect N-atom surface supercell, and $E^{\text{atom}}_{\text{bulk}}$ is the energy per atom in bulk Al.

The defective surfaces studied were 17-layer (100), 16-layer (111), and 15-layer (110). The concentration of the vacancy defect within the defective atomic layer is $\frac{1}{16}$ for all the slabs, which is more suitable for practical considerations of isolated defects than most of the known studies where the concentration was relatively high [11,51]. First, for the top two layers of the surfaces $E^{\text{s}}_{\text{form}}$ was calculated using the LDA, PBE, and PBEsol functionals, as reported in Table IV. These results are consistent with the surface energies as the $E^{\text{s}}_{\text{form}}$ for the topmost layer is in the order (111) > (100) > (110). In other words, the more stable a surface is, the higher is the energy required to create a vacancy on it. The $E^{\text{s}}_{\text{form}}$ for top two layers of LDA and PBEsol surfaces is very similar, while the PBE results are lower than the other two functionals. The $E^{\text{s}}_{\text{form}}$ predictions for the crucial (100) and (111) surfaces are significantly lower than the predictions made by semiempirical potentials [12]. Our PBE results for the top two Al(111) layers are in agreement with a recent study which used 7 atomic layers [10]. Table IV shows that the VFE on the topmost layer for this surface is as low as ∼0.11–0.15 eV, depending on the functional used. The lower predictions of VFE than the bulk value are interesting as they might cause greater vacancy concentration in the top layer, thereby affecting growth and diffusion mechanisms of the nanocrystals.

The central part of this work is the trend of $E^{\text{s}}_{\text{form}}$, studied as a function of vacancy depth for the three surfaces using the PBE functional, which is shown in Fig. 5. First, Fig. 5 agrees with intuition as it shows that the VFE at the topmost layer is lower than that in bulk for all the low-indexed surfaces. The bulk value is indicated by a dashed black line of $E^{f}_{vac} \sim 0.63$ eV. Markedly for the Al(111) subsurfaces, the $E^{\text{s}}_{\text{form}}$ is clearly always above the bulk line. However, within about six layer depths $E^{\text{s}}_{\text{form}}$ subsequently converges to the bulk-Al value within 10 meV. This nonmonotonous trend observed for the Al(111) surface is of interest from the point of view of concentration of vacancy defects. Contrary to the expectation,

TABLE IV. Vacancy formation energies (eV) for the top two layers (layer depth 00 and 01) for three low-indexed Al-surfaces.

$E^{\text{s}}_{\text{form}}$	LDA	PBE	PBEsol	Others
(100)–00	0.44	0.35	0.46	0.54,[a] 0.65[b]
(100)–01	0.75	0.68	0.80	1.19[a]
(110)–00	0.15	0.11	0.15	0.17,[a] 0.12[b]
(110)–01	0.57	0.52	0.61	1.16[a]
(111)–00	0.60	0.55	0.63	0.83,[a] 0.67,[b] 0.545[c]
(111)–01	0.72	0.66	0.77	1.12,[a] 0.66[c]

[a]EAM study [12].
[b]LDA study with energy cutoff of 108 eV and 8 Å vacuum [61].
[c]PBE study with 7 layers [10].

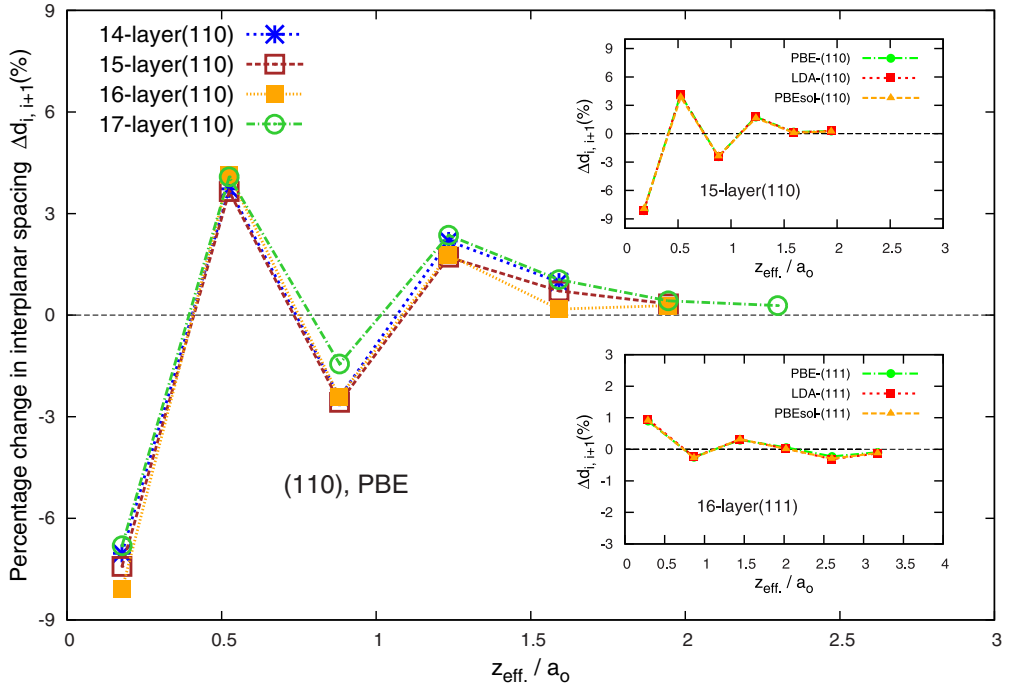

FIG. 4. For 14–17 layered (110) slabs, using the PBE functional, percentage change in the interlayer distance $\Delta d_{i,i+1}$ (%) of (110) surface is shown as a function of the slab depth which is given by $z_{\text{eff.}}/a_o$. In the inset: for 15-layer (110) (top) and 16-layer (111) (below), $\Delta d_{i,i+1}$ (%) is shown as a function of $z_{\text{eff.}}/a_o$ for different functionals.

the $E^{\text{s}}_{\text{form}}$ does not stabilize rapidly, and remains above the bulk line for the Al(111) surface. Owing to this, it can be speculated that the defect concentration can be possibly high for the topmost layer alone, and not for the subsurface layers. Certainly, for the case of nanocrystals with many edges and steps these trends may not be directly applicable. However, given that the (111) facets might represent significant surface areas on fcc metallic nanocrystals owing to their lowest surface energy, such a nonmonotonous trend in their VFEs is remarkable. The (110) surface is seen to converge fastest,

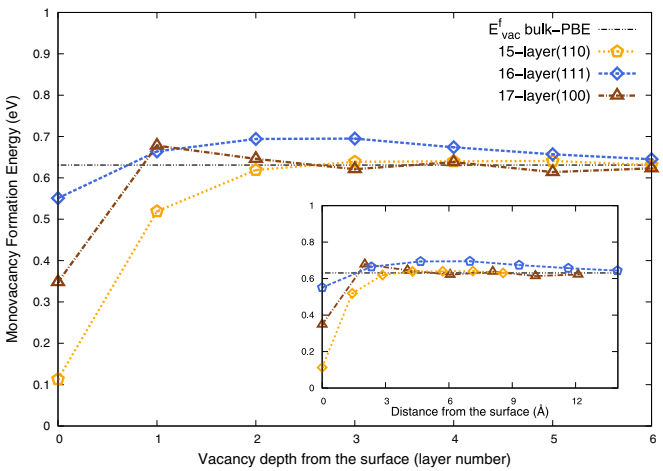

FIG. 5. Monovacancy formation energy as a function of vacancy depth for 17-layered (100), 16-layered (111), and 15-layered (110) surfaces, using GGA-PBE functional. Inset: the trend of $E^{\text{s}}_{\text{form}}$ with respect to the distance from the free surface is shown. Lines are used to guide the eye.

and monotonously, to the bulk value within a depth of three atomic layers. The behavior of (100) surface is intermediate between the other surfaces, and also converges after three layer depths.

In the inset of Fig. 5 the trend of $E^{\text{s}}_{\text{form}}$ is plotted as a function of distance from the free surface. The interlayer spacings of the three surfaces are $\frac{a}{2\sqrt{2}}$, $\frac{a}{2}$, and $\frac{a}{\sqrt{3}}$ for (110), (100), and (111), respectively. Our analysis covered a depth of 0–6 subsurface layers, and hence, the spanned distance from the surface up to which the defects are studied varies with each surface. The inset of Fig. 5 clearly shows the difference in convergence behavior where the (110) surface despite having the smallest interplanar spacing and least atomic planar density converges already at a smaller layer depth within 3 Å. On the other hand, although the (111) surface has the largest interplanar distance, it converges only beyond 11 Å. In this way, Fig. 5 indicates an inverse correlation of the rate of convergence of $E^{\text{s}}_{\text{form}}$ to the bulk value of E^{f}_{vac} with the packing density of a particular surface. To further understand these relations, we have investigated the relaxations of atomic planes, which will be further be discussed in Sec. III F.

E. Depth profile using different functionals

To compare the effect of exchange correlation functionals on these depth-dependence VFE profiles, we studied the Al(110) and Al(111) surfaces using the LDA and PBEsol functionals. The results are shown in Fig. 6, where 15-layer (110) and 16-layer (111) slabs are used for all the functionals. Figure 6 exhibits the nonmonotonous trend of $E^{\text{s}}_{\text{form}}$ of Al(111) for each of the three functionals. In fact, the VFE profiles for the three functionals are shifted from one another by their bulk

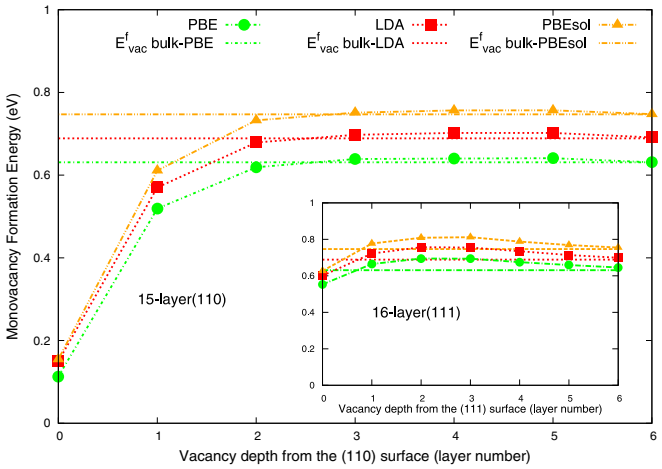

FIG. 6. Depth profile of vacancy formation energies for (110) and (111) Al surfaces using PBE, LDA, and PBEsol functionals.

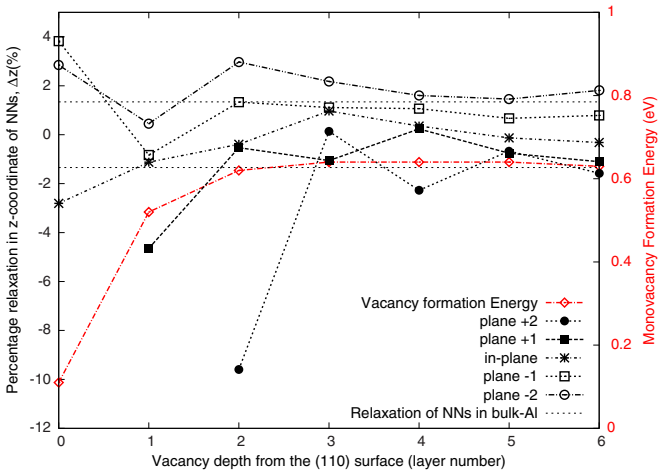

FIG. 7. Perpendicular relaxations of NNs of a vacancy defect in subsurface layers of Al(110).

values of Table II. Such a similarity in the effect of functionals can also be expected for Al(100) surfaces.

An interesting feature of Fig. 6 is that for a particular layer depth, the difference between the VFE for any two functionals is smaller for the topmost surface than that at subsequent depths, and remains almost unchanged after a depth of two layers. Also, Fig. 6 again highlights the similarity in the description of surfaces of LDA and PBEsol, whereas for deeper depths their behavior branches out to attain their respective bulk values. Assuming the conjecture that the description of point defects by different functionals is directly affected by their internal surface area [29–32], these trends can be readily explained. The internal surface area would be significantly larger for vacancy defects in the deeper subsurfaces than of the topmost surface. This would directly cause the difference in the intrinsic surface treatment of the functionals and, consequently, in the VFEs. The intrinsic surface treatment for a particular functional depends on the intrinsic surface correction per unit area $\sigma^{xc}_{cor}[n(r)]$ and the internal surface areas of the point defects. This internal surface area of the vacancy defect is known to be similar for different functionals [32], especially, as the lattice parameter predictions of these functionals are very close to each other for Al. Hence, the differences between functionals for a particular depth is directly proportional to the defect areas at that depth, which increases, and becomes constant within two layer depths. In this way, Fig. 6 indicates that the internal surface area of a defect plays a direct role in determining the VFEs, as earlier postulated [29–32].

F. Relaxations of nearest neighbors perpendicular to the surface

To understand the remarkable difference in the convergence behaviors of VFEs found for (110) and (111) surfaces, and how it depends on the packing density of a surface, we investigated the perpendicular relaxations of nearest neighbors (NN) for each configuration of a vacancy in a slab. For each configuration containing the vacancy in a subsurface layer, these relaxations are measured in terms of percentage relaxation of the NNs in the z direction, Δz (%), relative to the nearest-neighbor distance in fcc Al. The motivation to examine these relaxations comes from the fact that in pure surfaces the magnitude of interplanar relaxation $\Delta d_{i,i+1}$ is directly related to the packing density of the surfaces. For defected surfaces we choose to examine Δz, which also accounts for the relaxations of NN atoms, perpendicular to the surface. In this way, Δz in defective slabs with varying vacancy depths is an analog of the parameter $\Delta d_{i,i+1}$ used for pure surfaces.

The Δz analysis for Al(110) using the PBE functional is shown in Fig. 7. For the vacancy defect in the (110) subsurfaces, the NNs lie in the defect-containing layer, and the two planes below and above the defect. In Fig. 7, percentage z relaxations are plotted for each NN plane, for each depth of the monovacancy in the subsurface layers. For a particular vacancy depth, the relaxations corresponding to the nth NN plane are represented by plane $\pm n$, depending on whether the neighbors are in the layers above (+) or below (−) the defect. The dotted black lines represent the corresponding values of NN relaxation in bulk Al, which are included here for reference. On the right-hand axis, the depth profile of the VFEs is also shown for reference. It is found that the steep convergence seen in the top two layers is brought about by the large and opposite z relaxations of the in-plane and above-plane NNs. Interestingly, Δz of the NN in the planes above the defect (closer to the surface) are large and oscillatory even up to four layer depths. Such large relaxations of the NN planes of a defect, even for deep subsurfaces, accommodate the formation of vacancy defects. These trends in Fig. 7 indicate that the fast convergence of (110) surface towards a bulklike environment is facilitated by almost unhindered relaxations of its atomic planes, especially those above the defect.

A similar analysis is also shown for the Al(111) surface in Fig. 8. In this case, in addition to the atomic plane containing the defect, the NNs lie in the planes above and below it. First, we expect that the inherent structure of close-packed (111) planes would hinder the perpendicular relaxations of the atomic planes. This is seen for the defective slabs in Fig. 8, as the magnitude of z relaxations is significantly smaller ($\sim 1\%$). The close-packed (111) surface planes are restricted to relax in the direction perpendicular to the surface, and are ineffective to accommodate the created defect in the immediate subsurfaces.

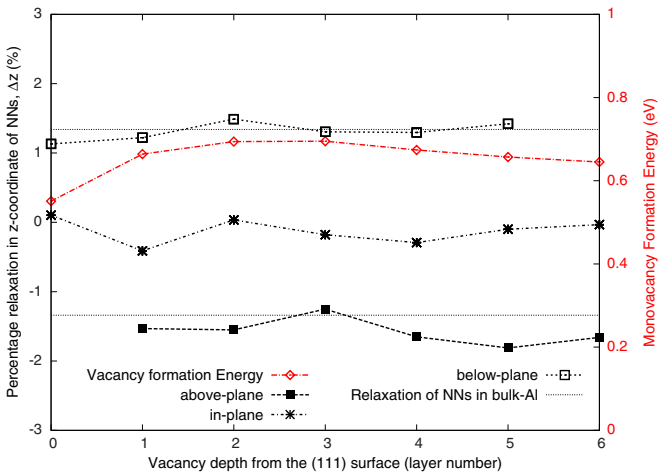

FIG. 8. Perpendicular relaxations of NNs of a vacancy defect in subsurface layers of Al(111).

This directly results into higher defect formation energy than that of bulk, and the slow convergence of Al(111) surface to the bulk value. This kind of *jamming* seen in the flat Al(111) surfaces, due to the steric interactions of its structure, cost the energy penalty for forming vacancies in the immediate (111) subsurfaces. Subsequently in the deeper subsurfaces, it is the relaxations of the atomic planes between the defect and the free surface which assist in converging of VFE to the bulk values, as in the case of Al(110).

IV. CONCLUSION

In this study, we have shown that depending on the crystallographic orientation the VFEs on low-indexed Al surfaces converge to a bulklike environment within a depth of 3–6 atomic layers. Furthermore, we show that within a depth of two subsurface layers, very similar LDA and PBEsol surfaces begin to exhibit differences in the electronic description of bulk Al. The depth dependence profile for VFEs of (110) and (111) surfaces is shown to be directly related to the steric interactions of atomic planes that determine the relaxations in the perpendicular direction, for a given surface. This implies that the surface-to-bulk transition of different surfaces is not determined by the distance from the surface, but by the atomic packing density of a given surface. The VFEs in the top layers of the surfaces are substantially lower than those in the interior of the nanocrystal. Interestingly, the defect formation energy of Al(111) shows a nonmonotonous trend in converging to the bulk value for all the chosen functionals, as the VFE for immediate subsurfaces is higher than that of bulk Al. For multifaceted Al nanocrystals one might expect a larger concentration of vacancy defects within the nanocrystals owing to higher surface to volume ratio. However, considering the predominance of (111) facets, our results indicate that the occurrence of vacancy defects in the immediate subsurfaces may actually be lower than the bulk Al. Nevertheless, the low VFEs on the topmost atomic planes for surfaces may play an important role for the growth and diffusion mechanisms at elevated temperatures.

ACKNOWLEDGMENTS

This work was funded by the Foundation for Fundamental Research on Matter (FOM) and the Netherlands Organization for Scientific Research (NWO) in the Industrial Partnership Programme Computational Sciences for Energy Research (Grant No. 13CSER067). This research programme is co-financed by Shell Global Solutions International B.V. M.A.v.H. acknowledges NWO for a VIDI (Grant No. 723.012.006). S.S.G. would like to thank the master students K. Perrier and A. van der Feltz for their initial work. Helpful suggestions on this manuscript by G. Avvisati and B. van der Meer are also gratefully acknowledged.

[1] J. P. Pierce, N. C. Bartelt, and K. F. McCarty, Phys. Rev. Lett. **99**, 026101 (2007).
[2] Y. He, O. Dulub, H. Cheng, A. Selloni, and U. Diebold, Phys. Rev. Lett. **102**, 106105 (2009).
[3] Y. Li and Y. Gao, Phys. Rev. Lett. **112**, 206101 (2014).
[4] A. S. Barnard, N. P. Young, A. I. Kirkland, M. A. van Huis, and H. Xu, ACS Nano **3**, 1431 (2009).
[5] R. van Gastel, E. Somfai, S. B. van Albada, W. van Saarloos, and J. W. M. Frenken, Phys. Rev. Lett. **86**, 1562 (2001).
[6] U. Aschauer, Y. He, H. Cheng, S.-C. Li, U. Diebold, and A. Selloni, J. Phys. Chem. C **114**, 1278 (2010).
[7] A. O. Yalcin, Z. Fan, B. Goris, W.-F. Li, R. S. Koster, C.-M. Fang, A. van Blaaderen, M. Casavola, F. D. Tichelaar, S. Bals, G. V. Tendeloo, T. J. H. Vlugt, D. Vanmaekelbergh, H. W. Zandbergen, and M. A. van Huis, Nano Lett. **14**, 3661 (2014).
[8] Z. Zanolli and J.-C. Charlier, Phys. Rev. B **81**, 165406 (2010).
[9] A. Kiejna, Phys. Rev. B **68**, 235405 (2003).
[10] Y. Zhu, W. Zheng, Y. Pan, Y. Pan, T. Liu, X. Zhou, D. Shi, Y. Shi, and X. Wei, Surf. Sci. **637–638**, 85 (2015).
[11] R. P. Kauffman and A. M. Rappe, Phys. Rev. B **67**, 085403 (2003).
[12] R. Li, Y. Zhong, C. Huang, X. Tao, and Y. Ouyang, Phys. B (Amsterdam) **422**, 51 (2013).
[13] S. Eremeev, A. Lipnitskii, A. Potekaev, and E. Chulkov, Russ. Phys. J. **40**, 276 (1997).
[14] Y.-N. Wen, Central Eur. J. Phys. **12**, 559 (2014).
[15] D. M. Ceperley and B. J. Alder, Phys. Rev. Lett. **45**, 566 (1980).
[16] J. P. Perdew and A. Zunger, Phys. Rev. B **23**, 5048 (1981).
[17] J. P. Perdew, K. Burke, and M. Ernzerhof, Phys. Rev. Lett. **77**, 3865 (1996).
[18] J. P. Perdew, A. Ruzsinszky, G. I. Csonka, O. A. Vydrov, G. E. Scuseria, L. A. Constantin, X. Zhou, and K. Burke, Phys. Rev. Lett. **100**, 136406 (2008).
[19] G. Kresse and J. Hafner, Phys. Rev. B **47**, 558 (1993).
[20] G. Kresse and J. Furthmüller, Comput. Mater. Sci. **6**, 15 (1996).
[21] G. Kresse and J. Furthmüller, Phys. Rev. B **54**, 11169 (1996).
[22] P. E. Blöchl, Phys. Rev. B **50**, 17953 (1994).
[23] H. J. Monkhorst and J. D. Pack, Phys. Rev. B **13**, 5188 (1976).
[24] M. Methfessel and A. T. Paxton, Phys. Rev. B **40**, 3616 (1989).

[25] R. Armiento and A. E. Mattsson, Phys. Rev. B **72**, 085108 (2005).
[26] W. Kohn and A. E. Mattsson, Phys. Rev. Lett. **81**, 3487 (1998).
[27] C. Varvenne, F. Bruneval, M.-C. Marinica, and E. Clouet, Phys. Rev. B **88**, 134102 (2013).
[28] M. H. F. Sluiter and Y. Kawazoe, Modell. Simul. Mater. Sci. Eng. **8**, 221 (2000).
[29] K. Carling, G. Wahnström, T. R. Mattsson, A. E. Mattsson, N. Sandberg, and G. Grimvall, Phys. Rev. Lett. **85**, 3862 (2000).
[30] T. R. Mattsson and A. E. Mattsson, Phys. Rev. B **66**, 214110 (2002).
[31] A. E. Mattsson, R. Armiento, P. A. Schultz, and T. R. Mattsson, Phys. Rev. B **73**, 195123 (2006).
[32] R. Nazarov, T. Hickel, and J. Neugebauer, Phys. Rev. B **85**, 144118 (2012).
[33] P. Vinet, J. Ferrante, J. R. Smith, and J. H. Rose, J. Phys. C: Solid State Phys. **19**, L467 (1986).
[34] R. Gaudoin, W. M. C. Foulkes, and G. Rajagopal, J. Phys.: Condens. Matter **14**, 8787 (2002).
[35] G. I. Csonka, J. P. Perdew, A. Ruzsinszky, P. H. T. Philipsen, S. Lebègue, J. Paier, O. A. Vydrov, J. G. Ángyán, Phys. Rev. B **79**, 155107 (2009), and references therein.
[36] M. Ropo, K. Kokko, and L. Vitos, Phys. Rev. B **77**, 195445 (2008).
[37] J. L. D. Silva, C. Stampfl, and M. Scheffler, Surf. Sci. **600**, 703 (2006).
[38] D. Simonovic and M. H. F. Sluiter, Phys. Rev. B **79**, 054304 (2009).
[39] A. E. Mattsson, R. Armiento, J. Paier, G. Kresse, J. M. Wills, and T. R. Mattsson, J. Chem. Phys. **128**, 084714 (2008).
[40] B. Medasani, M. Haranczyk, A. Canning, and M. Asta, Comput. Mater. Sci. **101**, 96 (2015).
[41] C. Kittel, *Introduction to Solid State Physics*, 8th ed. (Wiley, Hoboken, NJ, 2005), p. 704.
[42] L. Delczeg, E. K. Delczeg-Czirjak, B. Johansson, and L. Vitos, J. Phys.: Condens. Matter **23**, 045006 (2011).
[43] A. Glensk, B. Grabowski, T. Hickel, and J. Neugebauer, Phys. Rev. X **4**, 011018 (2014).
[44] K. M. Carling, G. Wahnström, T. R. Mattsson, N. Sandberg, and G. Grimvall, Phys. Rev. B **67**, 054101 (2003).
[45] P. Ehrhart, P. Jung, H. Schultz, and H. Ullmaier, *Atomic Defects in Metals*, 1st ed., edited by H. Ullmaier, Landolt-Börnstein-Numerical Data and Functional Relationships in Science and Technology-New Series, Vol. 25 (Springer, Berlin, 1991).
[46] N. E. Singh-Miller and N. Marzari, Phys. Rev. B **80**, 235407 (2009).
[47] C. Fang, M. A. van Huis, D. Vanmaekelbergh, and H. W. Zandbergen, ACS Nano **4**, 211 (2010).
[48] H. G. Yang, C. H. Sun, S. Z. Qiao, J. Zou, G. Liu, S. C. Smith, and G. Q. Cheng, Hui Ming Lu, Nature (London) **453**, 638 (2008).
[49] S. Kurth and J. P. Perdew, Phys. Rev. B **59**, 10461 (1999).
[50] S. Kurth, J. P. Perdew, and P. Blaha, Int. J. Quantum Chem. **75**, 889 (1999).
[51] H. M. Polatoglou, M. Methfessel, and M. Scheffler, Phys. Rev. B **48**, 1877 (1993).
[52] F. Boer, *Cohesion in Metals: Transition Metal Alloys* (North-Holland, Amsterdam, 1988).
[53] V. Fiorentini and M. Methfessel, J. Phys.: Condens. Matter **8**, 6525 (1996).
[54] H.Lüth, *Surfaces and Interfaces of Solid Materials*, 3rd ed. (Springer, Berlin, 1997).
[55] C. Herring, Phys. Rev. **82**, 87 (1951).
[56] M. W. Finnis and V. Heine, J. Phys. F: Met. Phys. **4**, L37 (1974).
[57] U. Landman, R. N. Hill, and M. Mostoller, Phys. Rev. B **21**, 448 (1980).
[58] S. P. Chen, A. F. Voter, and D. J. Srolovitz, Phys. Rev. Lett. **57**, 1308 (1986).
[59] A. G. Eguiluz, Phys. Rev. B **35**, 5473 (1987).
[60] J. R. Noonan and H. L. Davis, Phys. Rev. B **29**, 4349 (1984).
[61] R. Stumpf and M. Scheffler, Phys. Rev. B **53**, 4958 (1996).